Step Wandering Due to the Structural Difference of the Upper and the Lower Terraces

R. Kato[a]*, M. Uwaha[a] and Y. Saito[b]

[a]Department of Physics, Nagoya University
Furo-cho, Chikusa-ku, Nagoya 464-8602, Japan
[b]Department of Physics, Keio University,
3-14-1 Hiyoshi, Kohoku-ku, Yokohama 223-8522, Japan

*Corresponding author; Tel: (+81) 52 789 3533, Fax: (+81) 52 789 2928,

E-mail: katou@slab.phys.nagoya-u.ac.jp

Abstract

We consider the wandering instability of steps due to a gap in the lifetime of adatoms for evaporation on the upper and the lower terraces. Our study is meant to explain the step wandering observed in the growth of Si(111) surface near its structural transition temperature. With a linear stability analysis and Monte Carlo simulations, we show that the instability of an isolated step occurs in growth if adatoms on the upper terrace evaporate more easily than those on the lower terrace. For the instability of a vicinal face, additional features are considered as the motion of the phase boundary and the mass flow across it during the phase transformation. It is found that steps and phase boundaries wander in-phase with a rather well-defined periodicity when evaporation is weak. We compare the result with that for a system with a gap in the diffusion coefficient. The simulation results show that the first mechanism is more effective to make the wandering steps in-phase and that the second mechanism induces step wandering in a wider range of parameters.

Keywords Monte Carlo simulations, surface diffusion, silicon,
morphological instability, vicinal face

PACS codes 81.10.Aj, 47.20.Hw, 68.35.Fx

1 Introduction

Step wandering and bunching are the major morphological instabilities observed on a vicinal face of many kinds of crystals [1]. Among them, wandering is an instability for step fluctuations along the steps. When neighboring steps wander in-phase, the surface develops a wavy pattern perpendicular to the steps. The instability is most likely due to the asymmetry in the diffusion field of adatoms on the upper and the lower terraces [2]. So far two mechanisms have been studied as the origin of the asymmetry. One is the Ehrlich-Schwoebel (ES) effect [3, 4, 5, 6, 7, 8] and the other is the drift of adatoms by an external field [9, 10, 11].

In our previous paper, we reported another mechanism of a wandering instability due to the gap in diffusion coefficients of adatoms, D_s's, on the upper and the lower terraces [12]. The mechanism is thought to be relevant to the step instability observed on the Si(111) surface close to its structural phase transition point T_c [13]. At a high temperature Si(111) vicinal face is in 1×1 phase, but as it is cooled down, the reconstructed 7×7 structure appears at the top of each step edge even above T_c [14]. The 7×7 region spreads over the terrace toward the step-up direction as temperature is lowered to T_c. Therefore, the surface structures on the upper and the lower sides of the terrace are different in a narrow temperature range near T_c. Hibino et al. investigated the behavior of steps near the transition temperature [13] and found the step instability. They also found that the product $D_s c_{eq}^0$ of the diffusion coefficient D_s and the equilibrium adatom density c_{eq}^0 differ by a factor of ten on the upper (7×7) and on the lower (1×1) terraces [15]. However, it is difficult to decide experimentally which of the two, D_s or c_{eq}^0, gives the main contribution for the instability. We first studied the effect of the diffusion coefficient previously [12], and found

the wandering instability in growth, in qualitative agreement with the experiment [13].

On the other hand, equilibrium adatom densities on the 1×1 and the 7×7 terraces are known to be different. Yang and Williams [16] experimentally found that the total atom density of the 1×1 phase is 6 percent higher than that of the 7×7. They estimated the equilibrium density of adatoms per 1×1 unit cell to be $0.20 - 0.22$, which is comparable to the estimation 0.25 from the RHEED analysis [17]. Although the density of moving adatoms on the reconstructed 7×7 phase is not known, the observation of islands nucleated by quick cooling from above to below T_c [16] certainly implies that the moving adatoms on the 7×7 phase is less than those on the 1×1 phase.

The difference of the equilibrium adatom density is attributed to a gap in the lifetime of adatoms for evaporation on two surface phases. This density gap or the gap in the evaporation lifetime might give some influence on the step instability. We shall study whether it favors or suppresses the instability by means of analytic and simulational methods, and compare the step wandering caused by a gap in the lifetime with that caused by a gap in the diffusion coefficient. Our concern is the stability of a vicinal face in general, when two different phases coexist on a terrace and they have a gap in equilibrium adatom densities. Therefore, most of our study is concentrated on the generic features of a simplified model. Still, the results are sometimes compared with the experimental facts of the Si(111) surface to check the relevance of the model.

In **2** we introduce a simple model of a stepped surface with different structures on the upper and the lower terraces. There is only a single step in the system. By means of a linear stability analysis we derive a condition for the wandering instability of this isolated step. The theoretical analysis is compared to the result of Monte Carlo simulations for a single step in **3**. In **4** we extend our model to a vicinal face, where one has to consider phase boundaries between two steps as well. Steps and phase boundaries move by incorporating and releasing adatoms. They interact via elastic repulsion as well as via the diffusion field of adatoms. Linear stability analysis for this system is compared to Monte Carlo simulations.

Also, the behavior of steps is compared with that in a system with a gap in the diffusion coefficient. We give a discussion on our result in **5**.

2 Linear stability analysis of a single step

In this section we introduce a simple step flow model [18] with a single step on a surface, and derive the amplification rate of the wandering fluctuation by a linear stability analysis [5], similar to that of the previous paper [12].

2.1 The continuum model

The step separates the lower and the upper terraces on which adatoms have different lifetimes for evaporation, τ_1 and τ_2. Hereafter the subscript 1(2) indicates that the quantity is defined on the lower(upper) terrace. We assume in most of the paper that the diffusion coefficients on both terraces are the same ($D_1 = D_2 \equiv D_s$), unless we notify differently. Therefore the diffusion lengths x_1 and x_2 ($x_{1,2} = \sqrt{\tau_{1,2}\, D_s}$) are different. In the Si(111) surface, the lower terrace has the 1×1 structure with a longer lifetime than the upper terrace with the 7×7 structure: $\tau_1 > \tau_2$. In order to focus on the effect of the gap in the lifetime on the step instability, we want to suppress the ES effect. The suppression is achieved by the assumption of a perfectly permeable step [10, 19] (with a permeability $P = \infty$). Because of this assumption, solidification from the upper and from the lower terraces are indistinguishable.

The adatom density on the lower and the upper terraces $c_{1,2}(x, y, t)$ obeys the diffusion equation

$$\frac{\partial c_{1,2}}{\partial t} = D_s \nabla^2 c_{1,2} + f - \frac{c_{1,2}}{\tau_{1,2}} \ , \tag{1}$$

where f is the impingement rate of atoms. In our system we suppose that the step is parallel to the x axis on average and the y axis points toward the step-down direction. The difference of the adatom lifetime, τ_1 and τ_2, for evaporation should be related to a gap ΔE

in the adatom potential energy between the lower and the upper terraces, which is shown in Fig.1. We derive this relation as follows. The equilibrium on the upper and on the lower terraces should be established for a unique impingement rate of atoms f_{eq}. Since the adatom densities on the upper and the lower terraces are homogeneous in equilibrium, Eq.(1) tells us that their ratio equals to that of the adatom lifetimes;

$$f_{eq} = c^0_{eq1}/\tau_1 = c^0_{eq2}/\tau_2 \ . \tag{2}$$

On the other hand, in equilibrium chemical potentials of adatoms on both terraces should be equal to the chemical potential of an atom constituting the step edge of a crystal, μ^0_{eq}. Due to the gap ΔE in the adatom potential energy, the chemical potential can be written as $\mu^0_{eq} = k_B T \ln c^0_{eq1} = k_B T \ln c^0_{eq2} + \Delta E$ at a low adatom density. (When the adatom density is high, we have to be careful to exclude the double-occupancy of a site by multiple adatoms. The effect will be discussed in **3.2** in detail.) Thus the ratio of the adatom lifetimes on both terraces, which we denote α, are given by the potential energy gap

$$\alpha \equiv \tau_2/\tau_1 = e^{-\Delta E/k_B T} \ . \tag{3}$$

As for diffusion across the step, it must be compatible with the different equilibrium densities on both terraces. When an adatom jumps from the lower to the upper terrace, it must overcome the extra energy gap ΔE. The probability of this process $p_{1\to 2}$ is smaller than the opposite process $p_{2\to 1}$ by a Boltzmann factor

$$p_{1\to 2} = p_{2\to 1}\, e^{-\Delta E/k_B T} = p_{2\to 1}\, \alpha \ . \tag{4}$$

The reduction factor α will be used in the Monte Carlo simulation in the next section.

As for the boundary conditions at the step position $y = \zeta(x)$, we assume the continuity of the chemical potential is achieved due to the perfect permeability

$$\mu_1(x,y)\Big|_{y=\zeta+0} = \mu_2(x,y)\Big|_{y=\zeta-0} \ , \tag{5}$$

and the material conservation

$$-D_s \frac{\partial c_2}{\partial y}\Big|_{y=\zeta-0} + D_s \frac{\partial c_1}{\partial y}\Big|_{y=\zeta+0} = K\left(c_1(x,y) - c_{eq1}\right)\Big|_{y=\zeta+0} = \frac{V_n}{\Omega} \ , \tag{6}$$

where Ω ($\equiv a^2$) is the atomic area. Here $\mu_{1,2}$ are the adatom chemical potentials on the lower and the upper terraces, respectively and related to the adatom densities as $\mu_1 = k_B T \ln c_1$, $\mu_2 = k_B T \ln c_2 + \Delta E$. K is the kinetic coefficient of the step, and V_n is the normal velocity of the step. In Eq.(6) one uses the equilibrium adatom density on the lower terrace for a curved step c_{eq1} which includes the Gibbs-Thomson effect as

$$c_{eq1} = c^0_{eq1} + \frac{\Omega\, c^0_{eq1}}{k_B T}\tilde{\beta}\kappa \equiv c^0_{eq1} + \Gamma\kappa \ , \tag{7}$$

where $\tilde{\beta}$ is the step stiffness, κ the step curvature.

2.2 Condition for wandering instability

We consider if the wandering instability takes place during the step advancement or retardation. To obtain the adatom density on a terrace, we use the quasi-static approximation, $\partial c_{1,2}/\partial t = 0$ in solving Eq.(1). Then the density on the lower terrace varies exponentially with a relaxation length x_1 and that on the upper terrace with x_2.

The boundary conditions, Eqs.(5) and (6), determine the density profile completely, and the velocity v_0 of a steadily moving straight step is easily obtained as

$$v_0 = \Omega\, \frac{K {x_1}^2 (x_1 + x_2)(f - f_{eq})}{K {x_1}^2 + D_s(x_1 + x_2)} \ . \tag{8}$$

With a sinusoidal perturbation of a wave number k to the straight step $\zeta_0(t) = v_0 t$, the step position $\zeta(x,t)$ and the normal step velocity V_n are given by

$$\begin{aligned} \zeta(x,t) &= \zeta_0(t) + \delta\zeta(x,t) \\ &= v_0\, t + \delta\zeta_k\, e^{ikx+\omega(k)\,t} \ , \qquad (9) \\ V_n(x,t) \approx \partial\zeta/\partial t &= v_0 + \omega(k)\, \delta\zeta_k e^{ikx+\omega(k)\,t} \ , \qquad (10) \end{aligned}$$

where $\omega(k)$ is the amplification rate of the wandering fluctuation. Due to the step fluctuation $\delta\zeta$, the adatom density changes to

$$c_1(x,y,t) = \tau_1\, f - \frac{K {x_1}^4\,(f - f_{eq})}{D_s\{K {x_1}^2 + D_s(x_1 + x_2)\}}\, e^{-(y-\zeta_0)/x_1} + \delta c_{1k}\, e^{-\Lambda_{1k}(y-\zeta_0)}\, e^{ikx+\omega(k)\,t}$$

$$\text{for} \quad y > \zeta \ , \tag{11}$$

$$c_2(x,y,t) \;=\; \tau_2\, f - \frac{K{x_1}^2{x_2}^2\,(f-f_{eq})}{D_s\{K{x_1}^2 + D_s(x_1+x_2)\}}\, e^{(y-\zeta_0)/x_2} + \delta c_{2k}\, e^{\Lambda_{2k}(y-\zeta_0)}\, e^{ikx+\omega(k)\,t}$$

$$\text{for} \quad y < \zeta \ . \tag{12}$$

To satisfy the quasi-static form of Eq.(1), $\Lambda_{1k,2k}$ in Eqs.(11), (12) are

$$\Lambda_{1k,2k} \;=\; \sqrt{\frac{1}{{x_{1,2}}^2} + k^2} \tag{13}$$

$$\approx\; \frac{1}{x_{1,2}}\Big[1 + \frac{1}{2}(x_{1,2}\,k)^2 - \frac{1}{8}(x_{1,2}\,k)^4 \cdots\Big] \ , \tag{14}$$

where the second line is for the long wavelength limit ($kx_{1,2} \ll 1$).

Following the standard linear stability analysis [5], we derive the amplification rate $\omega(k)$ as

$$\frac{\omega(k)}{\Omega} \;=\; \frac{K^2{x_1}^4\,(x_1\Lambda_{1k} - x_2\Lambda_{2k})(f-f_{eq})}{\{K{x_1}^2 + D_s(x_1+x_2)\}\{K{x_1}^2 + D_s({x_1}^2\Lambda_{1k} + {x_2}^2\Lambda_{2k})\}}$$

$$-\,\Gamma\,\frac{D_sK({x_1}^2\Lambda_{1k} + {x_2}^2\Lambda_{2k})}{K{x_1}^2 + D_s({x_1}^2\Lambda_{1k} + {x_2}^2\Lambda_{2k})}\,k^2 \ , \tag{15}$$

With Eq.(14), $\omega(k)$ in the long wavelength limit is expressed as

$$\omega(k) = W_1(f,x_1,x_2)\,k^2 - W_2(f,x_1,x_2)\,k^4 \ , \tag{16}$$

$$W_1(f,x_1,x_2) \;=\; \Omega\,\frac{K(x_1+x_2)}{2\,\{K{x_1}^2 + D_s(x_1+x_2)\}^2}$$

$$\times\Big[K{x_1}^4(x_1-x_2)(f-f_{eq}) - 2\,\Gamma D_s\Big(K{x_1}^2 + D_s(x_1+x_2)\Big)\Big] \ , \tag{17}$$

$$W_2(f,x_1,x_2) \;=\; \Omega\,\frac{K^2{x_1}^2}{8\,\{K{x_1}^2 + D_s(x_1+x_2)\}^3}\Big[{x_1}^2({x_1}^2 - {x_2}^2)(f-f_{eq})$$

$$\times\Big\{K{x_1}^2({x_1}^2 + {x_2}^2) + D_s\Big(3\,({x_1}^3 + {x_2}^3) + x_1x_2(x_1+x_2)\Big)\Big\}$$

$$+\,4\,\Gamma D_s({x_1}^3 + {x_2}^3)\Big(K{x_1}^2 + D_s(x_1+x_2)\Big)\Big] \ . \tag{18}$$

If $W_1 > 0$, the amplification rate is positive, $\omega(k) > 0$, for the wave number k smaller than the critical value $k_c = \sqrt{W_1/W_2}$, and the step becomes unstable for the step wandering. The stability boundary is given by $W_1(f, x_1, x_2) = 0$, and the critical impingement rate $f_c(x_1, x_2)$ is derived from Eq.(17) as

$$f_c(x_1, x_2) = \frac{2\,\Gamma D_s\{K{x_1}^2 + D_s(x_1 + x_2)\}}{K{x_1}^4(x_1 - x_2)} + f_{eq}\ . \tag{19}$$

Fig.2 shows the region of a single step wandering, marked by W in the parameter space of the impingment rate f and the lifetime ratio $\alpha = \tau_2/\tau_1$. (Although W_2 in Eq.(18) becomes negative if $\alpha \gg 1$ and $f \gg f_{eq}$, higher order terms assure that $\omega < 0$ for large k and Eq.(19) is valid.) If the lifetime on the lower terrace is longer than that on the upper terrace ($\alpha \leq 1$), $x_1 \geq x_2$ and the growing step is unstable for $f_c < f$. In the opposite condition ($\alpha > 1$), $x_1 < x_2$ and a sublimating step is unstable for $f < f_c$. Hereafter, we consider the case $\alpha \leq 1$ ($\tau_1 \geq \tau_2$) which corresponds to the Si(111) case [16, 17].

3 Monte Carlo simulation: the lattice model

3.1 Algorithm

To go beyond the linear stability and to understand the surface morphology after the instability sets in, Monte Carlo simulation is an appropriate method. Here we describe the simulation model and the algorithm. A step is situated on the (001) surface of a simple cubic lattice with a solid-on-solid (SOS) restriction, that means the step position is a single-valued function of x. We call this an SOS step model on a square lattice. The lattice constant a is chosen as the unit of length. In the x-direction we assume a periodic boundary condition, and in the y-direction a helical boundary condition is assumed in order to adjust the height difference due to the step. It is similar to that of Ref.[7] except for the following: 1) the lifetimes of an adatom for evaporation on the upper and the lower terraces are different; 2) the algorithm for impingement to prohibit double-occupancy is modified; 3) the diffusion over the step is allowed.

The simulation algorithm runs as follows. We try impingement of f atoms randomly on a unit surface area in a unit time,[1] but only that on an empty site is accepted. After impingement trial, we select one atom from adatoms on the surface or from solid atoms at the step edge. If an adatom is selected, it moves to one of its four nearest neighbor sites unless the destination site is already occupied by another adatom. After each diffusion trial, time is increased by $\Delta t = (4N_a)^{-1}$ with N_a being the total number of adatoms on the surface. In this time unit, the diffusion coefficient is $D_s = 1$. For the diffusion from a site on the lower terrace to another on the upper terrace over the step, the acceptance ratio is set to α ($= \tau_2/\tau_1 = e^{-\Delta E/k_BT}$, smaller than unity in the simulation) to realize the gap in potential energy. Afterwards its evaporation is tried with an evaporation probability $\Delta t/\tau_1$ in the time interval Δt for an adatom on the lower terrace and with $\Delta t/\tau_2$ ($> \Delta t/\tau_1$) for an adatom on the upper terrace. If the evaporation trial fails and the atom chosen happens to touch the step from the lower side, it tries solidification with an acceptance probability $p_{\rm s} = [1 + e^{(\Delta E_{\rm s} - \phi)/k_BT}]^{-1}$. Here $\Delta E_{\rm s}$ is the change of step energy (the change of step perimeter length times the step energy ϵ per lattice constant), and ϕ is the energy gain due to solidification. If the selected atom is a step atom, melting is tried unless there is an adatom on top. The melting probability is $p_{\rm m} = [1 + e^{(\Delta E_s + \phi)/k_BT}]^{-1}$ and, if accepted, the step atom becomes an adatom and mobile.

In the following simulations, unless it is explicitly stated otherwise, the system size is 512×256, and other simulation parameters are $\epsilon/k_BT = 2.0$, $\phi/k_BT = 2.0$, $\tau_1 = 256$, which means $\tilde{\beta}/k_BT = 2.76$, $x_1 = 16$, $x_2 = 16\sqrt{\alpha}$. In the simulation we study the effect of the impingement rate f and the lifetime ratio α on the step stability and on the surface morphology.

[1] In practice, the impingement is performed every $20 - 40$ diffusion trials.

3.2 Modification to the continuum model

The continuum model described in the previous section is valid in the low density limit. To make a proper correspondence to the lattice model, special care should be taken if we deal with two kinds of surfaces with different lifetimes. In equilibrium, two conditions must be satisfied at the step. First, the amount of solidified adatoms and that of melted atoms are equal:

$$p_{\rm s}\, c^0_{eq1} = (1 - c^0_{eq2})\, p_{\rm m} \ . \tag{20}$$

The extra factor on the right hand side comes from our algorithm that the step atom cannot melt if there is an adatom on top. Secondly, the net adatom diffusion current over the step vanishes. Considering the potential gap between the upper and the lower terraces, this condition is achieved if

$$c^0_{eq1}\,(1 - c^0_{eq2})\,\alpha = c^0_{eq2}\,(1 - c^0_{eq1}) \ . \tag{21}$$

The equilibrium densities, $c^0_{eq1,2}$, on both terraces are determined by solving Eqs.(20) and (21), and they depend on the lifetime ratio $\alpha = \tau_2/\tau_1$.

To incorporate the prohibition of double-occupancy, Eqs.(20) and (21), in the continuum description, we modify Eq.(1) as

$$\frac{\partial c_{1,2}}{\partial t} = D_s \nabla^2 c_{1,2} + (1 - c_{1,2})\, f - \frac{c_{1,2}}{\tau_{1,2}} \ , \tag{22}$$

Then, an effective lifetime and an effective diffusion length are defined as,

$$\tilde{\tau}_{1,2} = \frac{\tau_{1,2}}{1 + \tau_{1,2}\, f} \ , \qquad \tilde{x}_{1,2} = \sqrt{\tilde{\tau}_{1,2}\, D_s} \ . \tag{23}$$

The equilibrium impingement rate is

$$f_{eq} = \frac{c^0_{eq1}}{\tau_1\,(1 - c^0_{eq1})} = \frac{c^0_{eq2}}{\tau_2\,(1 - c^0_{eq2})} \ . \tag{24}$$

When we compare simulation results with the continuum theory, we use these relations.

In addition, if $\alpha > 1$ (the adatom density on the upper terrace is higher than that on the lower terrace; the opposite case shown in Fig.1), we need to modify the boundary condition Eq.(5) in order to take into account the extra potential barrier for diffusion at the step. Adatoms diffusing from the upper terrace to the solidification site at the step must overcome the extra potential gap, which ammount to the reduction factor $1/\alpha$ for the diffusion. We treat the diffusion over the step separately using the lattice model picture and connect it to the continuum diffusion model. In a steady state approximation, the diffusion current on the left-hand side of the solidification site can be written as

$$\begin{aligned} -D_s \frac{\partial c_2}{\partial y}\Big|_{y=\zeta-0} &= \frac{D_s}{a}\left[\frac{1}{\alpha}c_2\left(1-c_1\right)-c_1\left(1-c_2\right)\right]\Big|_{y=\zeta} \\ &\simeq \frac{D_s}{a}\left[\frac{1}{\alpha}\left(c_2-c^0_{eq2}\right)\Big|_{y=\zeta-0}-\left(c_1-c^0_{eq1}\right)\Big|_{y=\zeta+0}\right], \end{aligned} \tag{25}$$

where the second line is valid near the equilibrium and $y = \zeta \pm 0$ indicate the lattice sites on the right and the left side on the step. The diffusion current on the upper terrace represented in the left-hand side of Eq.(25) should be equal to the current over the step to realize steady state. With Eq.(25), we derive the critical impingement rate f_c in the region of $\alpha > 1$ as shown in Fig.3(b) and (c). If $\alpha < 1$, a similar boundary condition is not necessary since the potential barrier is absent in this case and the correction is numerically negligible.

In Fig.3(a), if α is close to unity, the step will never be unstable for any positive values of f. We can also see a suppression of the wandering and recovery of the stable growth mode when the step velocity is very large. This wandering suppression is due to the diminishing gap in effective diffusion length $\tilde{x}_{1,2}$ as f increases. For $\alpha > 1$ the wandering instability of growing step occurs, which is absent in Fig.2. The high potential barrier prevents adatoms on the upper terrace to climb up to the solidification site so that atoms solidified are supplied from the lower terrace. Therefore the diffusion current flows opposite to the step motion resulting in a usual Mullins-Sekerka type wandering instability. We confirmed the wandering behavior of a single step both in growth with $f = 2.00 \times 10^{-3}$ and in sublimation with $f = 0$ for $\alpha = 20$.

3.3 Simulation results

Fig.4 shows the time development of a single step starting from a straight line at $y = 0$. In the figure, the upper part is the lower terrace and the lower part is the upper terrace. The bar in the top part of the figures indicates the characteristic wavelength $\lambda_{max} = 2\pi/k_{max}$ calculated from the peak of $\omega(k)$ in Eq.(15).

Fig.4(a)-(c) show the effect of the lifetime ratio α on the wandering pattern under the same impingement rate $f = 3.00 \times 10^{-3}$: (a) $\alpha = 0.1$, (b) $\alpha = 0.3$ and (c) $\alpha = 0.7$. The corresponding equilibrium and critical impingement rates are (a) $f_{eq} = 6.00 \times 10^{-4}$, $f_c = 1.03 \times 10^{-3}$, (b) $f_{eq} = 5.81 \times 10^{-4}$, $f_c = 1.27 \times 10^{-3}$, and (c) $f_{eq} = 5.49 \times 10^{-4}$, stable and no f_c. Clearly, the fluctuation diminishes as α increases. According to Fig.3(a), the straight step is always stable for $\alpha = 0.7$ as seen in Fig.4(c).

Fig.4(a) and (d),(e) show the influence of f on wandering pattern under the same adatom lifetime $\tau_1 = 256$ and the ratio $\alpha = 0.1$: (a) $f = 3.00 \times 10^{-3}$, (d) $f = 2.00 \times 10^{-3}$ and (e) $f = 0$. Both Fig.4(a) and (d) show wandering with $f > f_c = 1.03 \times 10^{-3}$ and the wandering fluctuation intensifies as the impingement rate increases from (d) to (a). In Fig.4(e) where $f = 0$ is smaller than $f_{eq} = 6.00 \times 10^{-4}$, the surface is sublimating and the step is receding downwards in the panel. The straight step is obviously stable.

Fig.4(f) shows the wandering pattern with a longer lifetime $\tau_1 = 1024$ ($x_1 = 32$) with $\alpha = 0.1$ and $f = 1.00 \times 10^{-3}$. Compared with the system with a shorter lifetime $\tau_1 = 256$ but with the same $\alpha = 0.1$, the equilibrium and the critical impingement rates decrease as $f_{eq} = 1.50 \times 10^{-4}$, $f_c = 2.01 \times 10^{-4}$, and one expects strong instability. Therefore, we simulated the step evolution without the SOS restriction. In fact, the wandering intensifies as the evaporation becomes weak. These features are in common with the wandering due to the gap in diffusion coefficient [12].

The step velocity for various impingement rate f in the simulation is shown in Fig.5 for the case of $\alpha = 0.1$, $\tau_1 = 256$ ($x_1 = 16$). According to Eq.(8), the unperturbed step velocity

v_0 should increase linearly with f as indicated by the dotted line in the figure. But due to the prohibition of double-occupancy restriction in the simulation, results agree rather well with the result obtained by the continuum model with modification Eq.(23) near equilibrium ($f_{eq} = 6.00 \times 10^{-4}$). At about the critical impingement rate ($f_c = 1.03 \times 10^{-3}$) the simulation result starts to deviate from the theory, indicating the speeding up due to the enhanced step fluctuation caused by the wandering instability [7]. When f becomes large, another effect may contribute to the accelaration, which will be discussed later in **4.4**.

4 Wandering in a vicinal face

4.1 A simple model of the vicinal face

We have so far studied the wandering instability of a single step that separates two different phases of surface reconstruction. We assumed that the width of both phases are much larger than the diffusion length, which is not always the case in reality. Wandering instability is observed [13] on a vicinal surface of Si(111), where the distance between steps is probably smaller than the diffusion length. In order to study this kind of systems, there are several new factors we should consider. There are neighboring steps, which interact via mechanical forces as well as via the diffusion field of adatoms. Between these steps there are phase boundaries, the position of which is another degree of freedom in the system. In our previous work [12], where only the gap in the diffusion coefficient is considered, we neglected this freedom and assumed that the phase boundary is at the center of each terrace. In the present study, we take account of the gap in the equilibrium adatom density in the two phases. Here we must consider the mass conservation more seriously since the phase transformation is inevitably associated with the density change.

The density of the 1×1 phase is 6 percent larger than that of the 7×7 phase [16] and the conversion of the 7×7 structure to the 1×1 structure requires incorporation of additional Si atoms at the phase boundary. Thus a phase boundary acts as a sink to the adatoms as the 1×1 phase expands. The phase boundary is also a source of elastic strain and interact with

the neighboring steps [21]. To take account these effects qualitatively we use the following simplified model. The phase boundary is looked upon as a step without the height difference that separates two different kinds of terraces. Like a step, the phase boundary advances (the 1×1 phase expands) when an adatom is incorporated to it, and recedes (the 7×7 phase expands) when an atom at the boundary is transformed to an adatom. The neighboring steps and phase boundaries interact mechanically via the elastic repulsion. We attribute the same stiffness, the same elastic interaction and the same kinetic properties to the steps and the phase boundaries. Then the model is an array of steps, in which the evaporation lifetime on the consecutive terraces alternates. In our simplified step model, the mass conservation and other properties are quantitatively very different from the real system, but we hope to find new features of the complex system where the growth and the phase transformation are coupled.

We consider a vicinal face in which the parallel steps are aligned with an average distance l at $y = \zeta_m(x)$, as shown in Fig.6. The mth terrace between the mth and the $(m+1)$th steps is divided by the phase boundary at $y = \xi_m(x)$ into two regions corresponding to the lower $(\zeta_m < y < \xi_m)$ and the upper $(\xi_m < y < \zeta_{m+1})$ terraces on which the adatom lifetimes are τ_1 and τ_2, respectively. We assume the phase boundary has the same mechanical and kinetic properties as that of the step. For example, the straight phase boundary provides an array of force monopoles as the straight step [20]. Then, between them a logarithmic repulsive interaction due to the elastic effect is assumed as

$$U(r) = Const - A \ln r \ , \tag{26}$$

where r is their separation and A is the intensity of the interaction. In the simulation with curved steps and phase boundaries, we replace r by the difference of the y coordinates at the same x, that is $\xi_m(x) - \zeta_m(x)$ etc. for simplicity.

When all the step distance is l and the width of the lower terrace is $d \equiv \xi_m - \zeta_m$, as

shown in Fig.6, the forces acting on the step F_s and on the phase boundary F_b are given by

$$F_s(d) = -F_b(d) = \frac{d}{dr}\Big(U(r) + U(l-r)\Big)\Big|_{r=d} = -A\left(\frac{1}{d} - \frac{1}{l-d}\right) . \tag{27}$$

The equilibrium adatom densities at the step and the phase boundary $c^s_{eq1,2}$, $c^b_{eq1,2}$ are functions of d and given as $c^{s,b}_{eq1,2} = c^{s,b\,0}_{eq1,2}[1 + \Omega(\tilde{\beta}\kappa - F_{s,b})/k_BT]$ where $c^{s\,0}_{eq1,2}$ and $c^{b\,0}_{eq1,2}$ are the equilibrium densities for the single step and the phase boundary, respectively.

The boundary conditions at the step are given by Eqs.(5) and (6). When the phase boundary advances at $\alpha < 1$, adatoms are incorporated in the phase boundary from the high potential region. The energy gain for incorporation is then high as $\phi + \Delta E$. Then adatoms diffusing from the lower terrace (high density region) to the incorporation site must overcome the extra potential, and the adatom current in the left-hand side of the phase boundary is given as

$$\begin{aligned} -D_s \frac{\partial c_1}{\partial y}\Big|_{y=\xi-0} &= \frac{D_s}{a}\left[\,\alpha\, c_1\,(1-c_2) - c_2\,(1-c_1)\,\right]\Big|_{y=\xi} \\ &\simeq \frac{D_s}{a}\left[\,\alpha\,(c_1 - c^{b\,0}_{eq1})\,\Big|_{y=\xi-0} - (c_2 - c^{b\,0}_{eq2})\,\Big|_{y=\xi+0}\right] , \end{aligned} \tag{28}$$

where α (< 1) indicates the reduction of the diffusion probability. Another boundary condition at the phase boundary is the mass conservation corresponding to Eq.(6):

$$-D_s \frac{\partial c_1}{\partial y}\Big|_{y=\xi-0} + D_s \frac{\partial c_2}{\partial y}\Big|_{y=\xi+0} = K_b\,(c_2 - c^b_{eq2})\,\Big|_{y=\xi+0} , \tag{29}$$

where K_b is the kinetic coefficient of the phase boundary.

4.2 Steady state

We first study the steady state in which both steps and phase boundaries remain straight, and grow or sublimate with an equal velocity v_0 and a distance d_0 ($< l$). By solving the diffusion equation (22) in the stationary approximation under the boundary conditions, Eqs.(5), (6), (28) and (29), we can calculate the step velocity $v_s(d)$ and the phase boundary velocity $v_b(d)$ as functions of d. The steady growth velocity v_0 and the lower terrace width

d_0 are determined by the relation, $v_0 \equiv v_s(d_0) = v_b(d_0)$, which can be accomplished only numerically.

The results for the lower terrace width d_0 and the velocity v_0 as functions of the impingement rate f in the steady state are shown in Fig.7 by the solid line for $\tau_1 = 1024$ ($x_1 = 32$) and by the dotted line for $\tau_1 = 256$ ($x_1 = 16$), with $\alpha = 0.1$, $l = 64$ and $A/k_BT = 1$. Open circles and triangles are the simulation results. The simulation results agree well with the theory for the case of $\tau_1 = 256$ (the dotted line and the open triangles). However, the deviation from the theoretical line becomes significant for the case of $\tau_1 = 1024$ (the solid line and the open circles). The start of the deviation from theory roughly coincides with the initiation of the wandering instability. Similar deviation is observed in the velocity of a single step in Fig.5.

Note that the width of lower terrace d_0 at equilibrium in Fig.7(a) is away from the half of the step distance l, at which the repulsive forces among the steps and the phase boundaries balance. The reason is that the adatom densities at 'the solidification site' for the step and the phase boundary are different. The nonlinear effect in the lattice model such as Eq.(21) further shifts the chemical balance expected from the simple formula $\mu = k_BT \ln c$. In a real system of Si(111), the width at equilibrium is determined by the surface energy difference of the 1×1 and the 7×7 phases in addition to the elastic strain near the step. The effect of the surface energy difference can be taken into our model by introducing an additional constant force acting on the phase boundary and by adjusting the equilibrium position of the phase boundary.

As f is increased from the equilibrium value f_{eq} by about one third in Fig.7(a), the width of lower terrace d_0 drops suddenly. At the same time, the velocity curve in Fig.7(b) shows a change of the slope. The width d_0 decreases because the step that exchanges atoms with the high density site can grow faster than the phase boundary that exchanges atoms with the low density site. The drastic change is simply due to the weak elastic repulsion at the large step-phase boundary separation. When they are far apart, a small change in the force

balance can only be compensated by a large change in their distance.

Thus in our model the low density phase expands when the impingement (supersaturation) is increased in steady growth. Recently, Hannon et al. investigated the influence of an external flux on the multistructural Si(111) surface [22]. They observed that the higher the supersaturated flux of Si is, the larger the 1×1 area fraction is. When the flux is removed, the original configuration is almost recovered. Superficially, their observation contradicts our results. In the experiment, however, the system is not in a steady state and the steps do not seem to move; the increase of adatoms only shifts the phase boundary to reduce the number of adatoms. In our simplistic model, the phase boundary and the step are treated on the equal footing: they grow at the expense of the same amount of adatoms. Certainly, this is not true in Si(111). The phase boundary, which requires only 6 percent excess atoms, is much more sensitive to the supersaturation than steps. In order to compare with the experiment, a more elaborate model than the present one is required.

4.3 Wandering instability

For the vicinal face we perform a linear stability analysis similar to that in **2.2**. Since the calculation is very complicated, we only derive the amplification rate of an in-phase fluctuation where all steps and phase boundaries fluctuate in-phase. The mth step and the phase boundary are displaced from the straight steady state as

$$\zeta_m(x,t) = v_0\, t + m\, l + \delta\zeta_k\, e^{ikx+\omega(k)\, t}\ , \tag{30}$$

$$\xi_m(x,t) = v_0\, t + m\, l + d_0 + \delta\xi_k\, e^{ikx+\omega(k)\, t}\ . \tag{31}$$

When the step and the phase boundary have a curvature κ, the forces acting on them are given as $F_{s,b}(d_0) - \tilde{\beta}\kappa$ because we have assumed their stiffnesses are the same.

The growth rate of the fluctuation $\omega(k)$ is calculated numerically and shown in Fig.8 with $\alpha = 0.1$, $\tau_1 = 1024$ ($x_1 = 32$) and $A/k_BT = 1$. Fig.8(a) shows the effect of the impingement rate f with the fixed inter-step distance $l = 64$, and Fig.8(b) shows the effect of the inter-step distance l with the fixed impingement rate $f = 1.00 \times 10^{-3}$. The critical impingement

rate f_c is calculated as $f_c = 0.37 \times 10^{-3}$ in the condition of Fig.8(a) and this value coincides roughly with the one at which the simulation result of the lower terrace width d starts to deviate from the theory as shown in Fig.7. We can see from Fig.8(b) that the wandering instability is suppressed as the terrace width decreases since the effective cutoff length for adatom diffusion is decreased from $x_{1,2}$ to l.

Fig.9 shows a snapshot of the vicinal face, where the solid and the dotted lines represent the steps and the phase boundaries, respectively. The steps and the phase boundaries move in pairs, but the fluctuation of the array of pairs is not in-phase because of relatively long inter-step distance $l = 64$ compared with the diffusion lengths $x_1 = 32$. We traced the emergence of such wandering morphology starting from an equidistant array of straight steps and phase boundaries. Given the supersaturation ($f > f_c > f_{eq}$), the lower terrace width d decreases gradually. This narrowing of the lower terrace itself is expected from the steady state analysis in **4.2** and from Fig.7. Since the phase boundary has the low adatom density region in front and the high adatom density region in back, it must be stable against wandering when it advances as long as the lower terrace has sufficient width d. However, when d becomes too small, wandering instability of the phase boundary at a short wavelength seems to start. The adatom current to the phase boundary from the low adatom density region in front becomes dominant because the high density region in the back gets narrow. As a result, the wandering instability becomes possible in growth at the phase boundary. Thus the cause of the phase boundary wandering at a short wavelength in Fig.9 may be the very narrow back terrace. If so, the mechanism is in common with the instability on Si(111) reported by Homma et al. [23].

In Fig.10 we show the wandering pattern under weak evaporation condition ($x_{1,2}/l \gg 1$), which is realized in the temperature range of the Si(111) surface structural transition. In the experiment [13], wandering steps move in-phase and show an almost periodic pattern. The parameters in Fig.10 are $\alpha = 0.1$, $\tau_1 = 16384$ ($x_1 = 128$), $f = 3.00 \times 10^{-3}$ and the inter-step distance is $l = 64$ in (a), $l = 32$ in (b) and $l = 16$ in (c). In contrast to the

morphology under $x_{1,2}/l < 1$ in Fig.9, in-phase wandering patterns emerge except with the very small l (Fig.10.(c)), where the instability is suppressed for the short cutoff l. In addition to the short wavelength instability of the phase boundaries, the steps and the phase boundaries move in pairs and exhibit the in-phase wandering instability at a longer wavelength. Since two instabilities, the in-phase long-wavelength wandering and a short-wavelength phase-boundary wandering seem to coexist, the quantitative comparison with the theory is difficult.

In summary, the periodic in-phase wandering takes place in an intermediate inter-step distance range, where the step distance is shorter than the diffusion lengths but not too short to suppress wandering itself.

4.4 Alternating diffusion coefficient

In the previous paper [12] we studied the step wandering due to the gap in diffusion coefficient. But there, the incorporation and the release of adatoms are not considered at the phase boundary. Instead, the position of the phase boundary is automatically placed at the center of each terrace as $\xi_m = (\zeta_{m+1} + \zeta_m)/2$, for simplicity. For the comparison to the model so far presented in this paper, we need to consider the motion of the phase boundary independently in the case with a gap in the diffusion coefficient. Therefore, in the model in this subsection, the adatom lifetime for evaporation τ is set uniform on the surface, but the diffusion coefficients $D_{1,2}$ are taken different on the lower and the upper terraces. Such a situation is depicted schemtically in terms of a surface potential energy in Fig.11. The energy takes the same minimum value on both phases, 1 and 2, but the energy maximum or the surface diffusion barrier is different in phases 1 and 2. The diffusion lengths on the lower and the upper terraces $x_{1,2}$ are different again as $x_{1,2} = \sqrt{\tau D_{1,2}}$. The diffusion equation in the static approximation is

$$D_{1,2}\nabla^2 c_{1,2} + f - \frac{c_{1,2}}{\tau} = 0 \ . \tag{32}$$

The boundary conditions at the step, derived in the same way as Eqs.(28) and (29), are given as

$$-D_2 \left.\frac{\partial c_2}{\partial y}\right|_{y=\zeta-0} \simeq \frac{D_2}{a} \left(\left. c_2 \right|_{y=\zeta-0} - \left. c_1 \right|_{y=\zeta+0} \right) , \tag{33}$$

$$-D_2 \left.\frac{\partial c_2}{\partial y}\right|_{y=\zeta-0} + D_1 \left.\frac{\partial c_1}{\partial y}\right|_{y=\zeta+0} = K \left(\left. c_1 \right|_{y=\zeta+0} - c^s_{eq} \right) . \tag{34}$$

The boundary conditions at the phase boundary are

$$-D_1 \left.\frac{\partial c_1}{\partial y}\right|_{y=\xi-0} \simeq \frac{D_2}{a} \left(\left. c_1 \right|_{y=\xi-0} - \left. c_2 \right|_{y=\xi+0} \right) , \tag{35}$$

$$-D_1 \left.\frac{\partial c_1}{\partial y}\right|_{y=\xi-0} + D_2 \left.\frac{\partial c_2}{\partial y}\right|_{y=\xi+0} = K \left(\left. c_2 \right|_{y=\xi+0} - c^b_{eq} \right) , \tag{36}$$

where $c^{s,b}_{eq}$ are the equilibrium adatom density at the step and the phase boundary. In Eqs.(33) and (35), diffusion across the step and the phase boundary is treated separately to accomodate the possible density gap.

From the steady state solution we can calculate the velocity v_0 and the lower terrace width d_0. The results are shown in Fig.12 with $D_2/D_1 = 0.1$, $l = 64$ and $A/k_BT = 1$. The dotted lines represent the theoretical values with $\tau = 1024$ ($x_1 = 32$) and $\tau = 256$ ($x_1 = 16$). The open circles and the triangles are the simulation results. The lower terrace width at equilibrium is $d_0 = l/2$, where the repulsive forces balance. When f is increased the step, which exchanges atoms with the site on a fast diffusion tarrace, advances faster than the phase boundary and d decreases. A linear stability analysis similar to that in **4.3** predicts the critical impingement rate $f_c = 0.23 \times 10^{-3}$ for $x_1 = 32$ and $f_c = 0.83 \times 10^{-3}$ for $x_1 = 16$. The deviation of the simulation results from the theoretical line starts near f_c, as is shown in Fig.12(a). The deviation from the steady state solution near the instability point seems universal, as it is also observed in Fig.7 for a model with different lifetimes. However, the increase of d in the present case is very large and it finally saturates at large f. These behaviors cannot simply be attributed to the acceleration caused by the wandering. Since

f is much larger than f_c, the step velocity is large, and the static approximation Eq.(32) is no longer valid. We thus adopt a steady state approximation, in which the diffusion field is steady in the reference frame of the moving steps

$$D_{1,2}\nabla^2 c_{1,2} + v_0 \frac{\partial c_{1,2}}{\partial y} + f - \frac{c_{1,2}}{\tau} = 0 \ , \tag{37}$$

The characteristic length of the density variation in forward and backward directions are

$$\lambda_{1,2\pm}{}^{-1} = \sqrt{x_{1,2}{}^{-2} + l_{D\,1,2}{}^{-2}} \pm l_{D\,1,2}{}^{-1} \ , \tag{38}$$

where $l_{D\,1,2} \equiv 2D_{1,2}/v_0$ is the ordinary diffusion length on the lower and the upper terraces and the subscript $+(-)$ indicates the forward (backward) direction. When growth is fast the density profile of adatoms becomes highly asymmetric (note $\lambda_{1,2+} < \lambda_{1,2-}$ and the density in each region in Fig.11 is higher at the left-hand side than at the right-hand side). Due to the slow diffusion, the density on the upper terrace becomes high, and the phase boundary with the highest density region in front can move fast. In fact, similar to **4.2**, we can calculate d_0 and v_0 and the results are shown with solid lines in Fig.12. For the case of $x_1 = 16$, the calculation agrees with the simulation results very well. The calculation for the case of $x_1 = 32$ reproduces the increase of d, however, it overshoots the simulation results. The nonlinear terms in the boundary condition Eq.(36), which we have neglected may be the origin of the discrepancy.

We have also calculated d_0 and v_0 in the steady state approximation for Fig.7. The correction is small and negligible because the asymmetry in the adatom density profile is much less important when the density gradient is small (see Fig.14).

Snapshots of a vicinal face with the parameters $D_2/D_1 = 0.1$, $f = 3.00 \times 10^{-3}$, $\tau = 16384$ ($x_1 = 128$) are shown in Fig.13. The inter-step distance l is (a) $l = 64$, (b) $l = 32$ and (c) $l = 16$. The critical impingement rate f_c calculated with Eqs.(33)-(36) is (a) $f_c = 0.60 \times 10^{-4}$, (b) $f_c = 2.40 \times 10^{-4}$, (c) $f_c = 5.90 \times 10^{-4}$. The evaporation is weak and the result can be compared with that of Fig.10. The phase boundary is nearly at the middle of the terrace $d \sim l/2$ if the step distance is large (in (a) and (b)). In contrast to the result of Fig.10,

the periodic in-phase step wandering becomes evident as the terrace width decreases. Due to the introduction of the motion of the phase boundary, the wandering pattern looks less regular than our previous result [12], but the main features of wandering remain and agree with the experiment [13].

5 Conclusion and discussion

We studied the possibility of step wandering due to the gap of adatom lifetime for evaporation on the upper and the lower terraces, and compared the result with that due to a gap in the diffusion coefficient. The system corresponds to a Si(111) surface near the $1 \times 1 \leftrightarrow 7 \times 7$ structural transition temperature. Our model distinguishes two extreme cases, in which either the evaporation lifetime or the diffusion coefficient is different on the two phases. It is proposed to find out the major mechanism responsible for the step wandering on a Si(111) surface. The model takes the density change in the phase transformation into account and exhibits the interplay of crystal growth and the phase transformation. The density change in the present model is, however, very much exaggerated in comparison with the Si(111) surface.

We found that a growing step shows wandering instability above a critical impingement rate if adatoms evaporate more easily from the upper terrace than from the lower terrace: ($\alpha = \tau_2/\tau_1 < 1$). This conclusion agrees with experiment that the adatom density is higher on the 1×1 phase [17, 16] and the wandering instability occurs in growth [13]. We found no significant difference in the behavior of a single step for a system with different lifetimes compared with a system with different diffusion coefficients on two phases [12]. In the vicinal face of our model, as the supersaturation is increased and the crystal grows, the width of the high adatom density region (with a long lifetime) decreases so that the step and the phase boundary advance in pairs. The apparently opposite behavior, that is the enhancement of the 1×1 region with supersaturation, is observed in the experiment [22]. The discrepancy may be due to the exaggeration of the density change in the phase transformation in our

model.

We compared the simulation result of a system with different lifetimes with that with different diffusion coefficients. In Fig.14 we show the theoretical density profile of adatoms in the two models (in the static approximation). In the first model with different lifetimes, a large density gap at the phase boundary as well as at the step edge is evident. In the second model with different diffusion coefficient, the density is higher in the upper terrace. Under weak evaporation condition, the step and the phase boundary move in-phase and the periodic wandering pattern is realized in both cases. If the step distance l is very small ($l \ll x_2$), however, the wandering tends to be suppressed because the density variation extends only to a short distance l. The suppression of wandering is stronger in the system with different lifetimes, since the low density region in front of the phase boundary is narrow and diffusion current from the back seems to compensate the destabilizing effect.

In this paper we showed that both factors, a gap in the adatom lifetime and a gap in the diffusion coefficient, cause in-phase step wandering in growth if evaporation is weak. In the simulation, we observed that the first factor is more effective to make the wandering steps in-phase and that the second factor induces step wandering in a wider range of parameters. Unfortunately, the large density change during phase transformation in our model is unrealistic and it is not possible to compare our result directly with the Si experiment. At present we cannot conclude whether the wandering instability in Si(111) is mainly due to the effect of the gap in the diffusion coefficient or that in the lifetime.

However a good correspondence between the continuum model for the theoretical calculation and the lattice model for the simulation are accomplished by finding proper boundary conditions of the diffusion equation. This fact is quite meaningful because we can use these relations to study more realistic system, for example Si(111) with appropriate physical parameters, in a subsequent study.

Aknowledgements

The work is supported by the Grant-in-Aid for Scientific Research from Japan Society for the Promotion of Science. M. U. and Y. S. benifited from the Interuniversity Cooperative Research Program of the Institute for Materials Research, Tohoku University.

References

[1] For a recent review: K. Yagi, H. Minoda, M. Degawa, Surf. Sci. Rep. 43 (2001) 45.

[2] M. Uwaha, Y. Saito and M. Sato, J. Cryst. Growth 146 (1995) 164; M. Uwaha, M. Sato, Surf. Rev. Lett. 5 (1998) 841; M. Uwaha, in Fundamentals and Applications of Crystal Growth Research and Technology, edited K. Sato, K. Nakajima and Y. Furukawa (Elsevier, Amsterdam, 2001), pp. 78-99.

[3] G. Ehrlich, F. Hudda, J. Chem. Phys. 44 (1966) 1039.

[4] R. L. Schwoebel, E. J. Shipsey, J. Appl. Phys. 37 (1966) 3682.

[5] G. S. Bales, A. Zangwill, Phys. Rev. B 41 (1990) 5500.

[6] M. Uwaha, Y. Saito, Phys. Rev. Lett. 68 (1992) 224.

[7] Y. Saito, M. Uwaha, Phys. Rev. B 49 (1994) 10677.

[8] A. Pimpinelli, I. Elkinani, A. Karma, C. Misbah, J. Villian, J. Phys. Condens. Matter 6 (1994) 2661.

[9] M. Sato, M. Uwaha, J. Phys. Soc. Jpn. 65 (1996) 2146.

[10] M. Sato, M. Uwaha, Y. Saito, Phys. Rev. B 62 (2000) 8452.

[11] A. Natori, N. Suga, Appl. Surf. Sci. 190 (2002) 96.

[12] R. Kato, M. Uwaha, Y. Saito, H. Hibino, Surf. Sci. 522 (2003) 64.

[13] H. Hibino, Y. Homma, M. Uwaha, T. Ogino, Surf. Sci. 527 (2003) L222.

[14] N. Osakabe, Y. Tanishiro, K. Yagi, G. Honjo, Surf. Sci. 109 (1981) 353.

[15] H. Hibino, C.-W. Hu, T. Ogino, I. S. T. Tsong, Phys. Rev. B 63 (2001) 245402.

[16] Y.-N. Yang, E.D. Williams, Phys. Rev. Lett. 72 (1994) 1862.

[17] S. Kohmoto, A. Ichimiya, Surf. Sci. 223 (1989) 400.

[18] W. K. Burton, N. Cabrera, F. C. Frank, Phil. Trans. Royal Soc. London, 243 (1951) 299.

[19] M. Ozdemir, A. Zangwill, Phys. Rev. B 45 (1992) 3718.

[20] O. L. Alerhand, D. Vanderbilt, R. D. Meade, J. D. Joannopoulos, Phys. Rev. Lett. 61 (1988) 1973.

[21] J. B. Hannon, J. Tersoff, R. M. Tromp, J. Cryst. Growth 237-239 (2002) 181.

[22] J. B. Hannon, J. Tersoff, M. C. Reuter, R. M. Tromp, Phys. Rev. Lett. 89 (2002) 266103.

[23] Y. Homma, P. Finnie, M. Uwaha, Surf. Sci. 492 (2001) 125.

Fig.1: Schematic potential diagram for adatom diffusion on the surface. In this figure, adatoms on the upper terrace evaporate more easily than those on the lower terrace. a represents the lattice constant.

Fig.2: The critical impingement rate f_c (solid lines) and the equilibrium one f_{eq} (dashed line) as a function of $\alpha = \tau_2/\tau_1$ for $x_1 = 16$. W indicates wandering.

Fig.3: The critical impingement rate f_c (solid lines) and the equilibrium one f_{eq} (dashed lines) as a function of α for $x_1 = 16$ with the modifications Eq.(23).

Fig.4: The time development of a single step position. The parameters are (a) $(\alpha, f) = (0.1,\ 3 \times 10^{-3})$, (b) $(\alpha, f) = (0.3,\ 3 \times 10^{-3})$, (c) $(\alpha, f) = (0.7,\ 3 \times 10^{-3})$, (d) $(\alpha, f) = (0.1,\ 2 \times 10^{-3})$, (e) $(\alpha, f) = (0.1,\ 0)$ with $\tau_1 = 256$, $(x_1 = 16)$ and (f) $(\alpha, f) = (0.1,\ 1 \times 10^{-3})$ with $\tau_1 = 1024$, $(x_1 = 32)$.

Fig.5: Dependences of the step velocity v_0 on the impingement rate f. The solid and the dotted lines are from Eq.(8) with and without Eq.(23).

Fig.6: Schematic potential diagram for adatom diffusion on a vicinal surface. l is the inter-step distance, d the lower terrace width.

Fig.7: The lower terrace width d_0 (a) and the velocity v_0 (b) in the steady state as a function of the impingement rate f. Parameters are $\alpha = 0.1$, $l = 64$, $A/k_BT = 1$. The arrows indicate the equilibrium and the critical values of f.

Fig.8: The amplification rate with $\alpha = 0.1$, $\tau_1 = 1024$ $(x_1 = 32)$, $A/k_BT = 1$. (a) The effect of impingement rate f with the fixed value of $l = 64$. (b) The effect of inter-step

distance l with the fixed value of $f = 1.00 \times 10^{-3}$.

Fig.9: Snapshot of a vicinal face with $\alpha = 0.1$, $f = 1.00 \times 10^{-3}$, $\tau_1 = 1024$ ($x_1 = 32$). The inter-step distance l is $l = 64$.

Fig.10: Snapshots of a vicinal face with $\alpha = 0.1$, $\tau_1 = 16384$ ($x_1 = 128$), $f = 3.00 \times 10^{-3}$. Inter-step distance is $l = 64$ in (a), $l = 32$ in (b), $l = 16$ in (c). The system size is 512×128.

Fig.11: Schematic potential for adatom on the surface with the gap in diffusion coefficient. Adatoms on the lower terrace diffuse more easily.

Fig.12: The lower terrace width d_0 (a) and the velocity v_0 (b) in the steady state of a vicinal face as a function of f. Parameters are set to $D_2/D_1 = 0.1$, $l = 64$, $A/k_BT = 1$. The arrows indicate the equilibrium and the critical values of f.

Fig.13: Snapshots of a vicinal face with $D_2/D_1 = 0.1$, $f = 3.00 \times 10^{-3}$, $\tau = 16384$ ($x_1 = 128$). The inter-step distance l is (a) $l = 64$, (b) $l = 32$, (c) $l = 16$. Note that the vertical size is enlarged. The system size is 512×128.

Fig.14: Steady state density of adatoms in the continuum model with $f = 1.00 \times 10^{-3}$, $l = 16$ and $\tau(\tau_1) = 1024$. (a) different lifetime, (b) different diffusion coefficient.

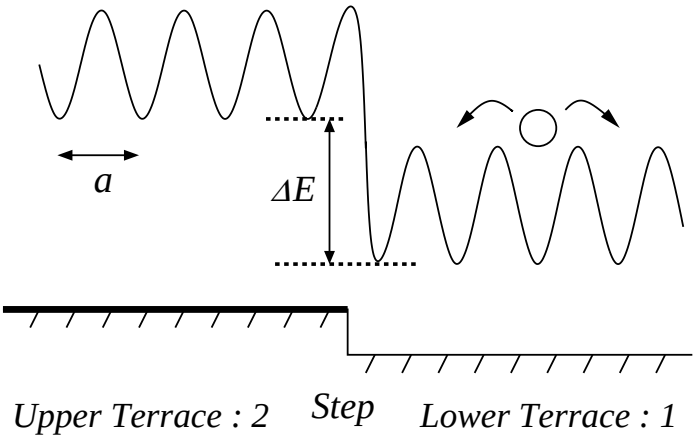
a
ΔE
Upper Terrace : 2
Step
Lower Terrace : 1

Fig.1

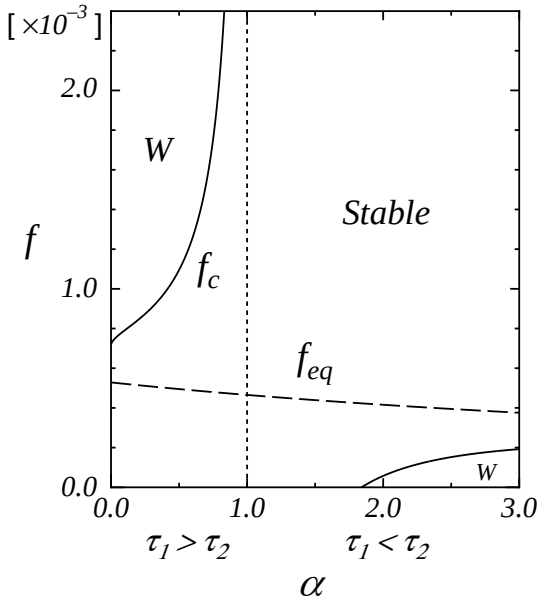
[×10^-3]
2.0
1.0
0.0
f
W
Stable
f_c
f_eq
W
0.0
1.0
2.0
3.0
τ1 > τ2
τ1 < τ2
α

Fig.2

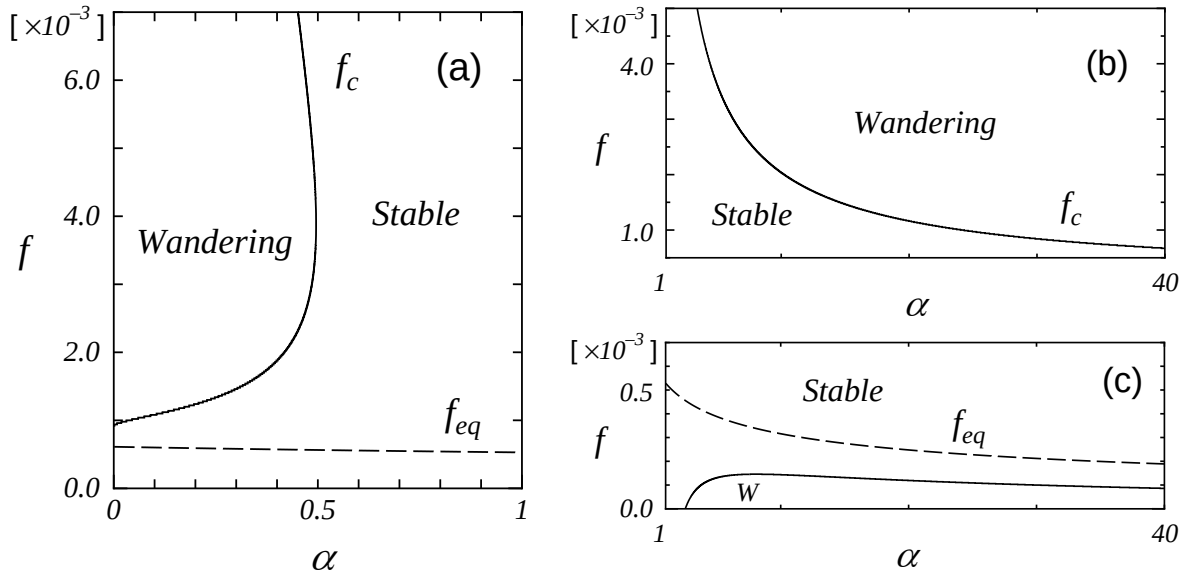

Fig.3(a),(b),(c)

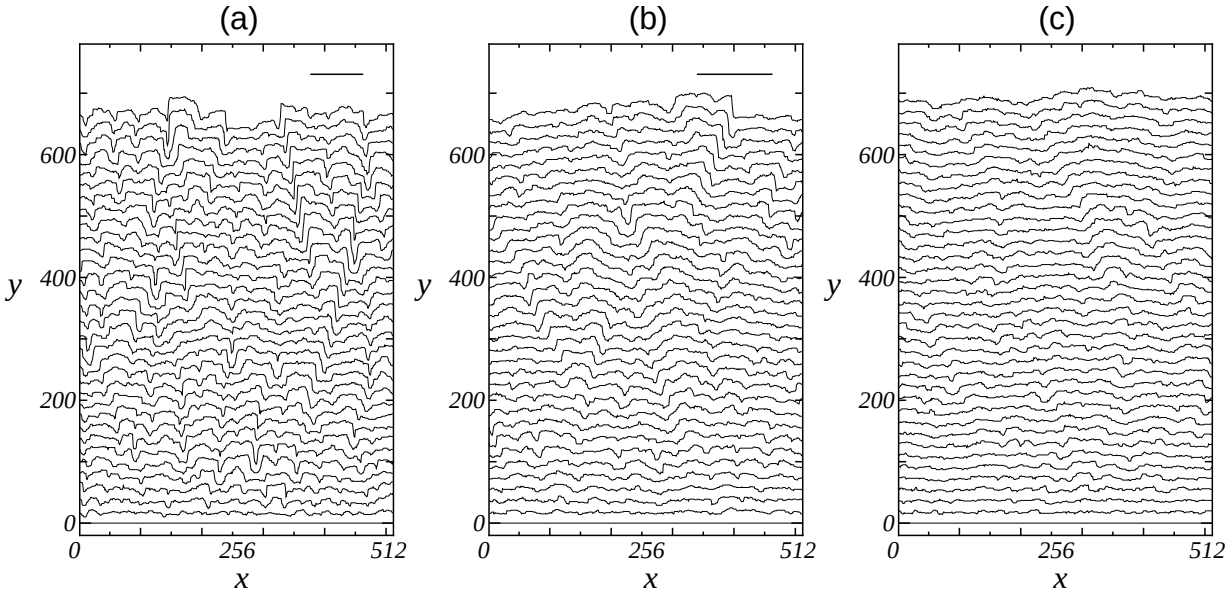

Fig.4(a),(b),(c)

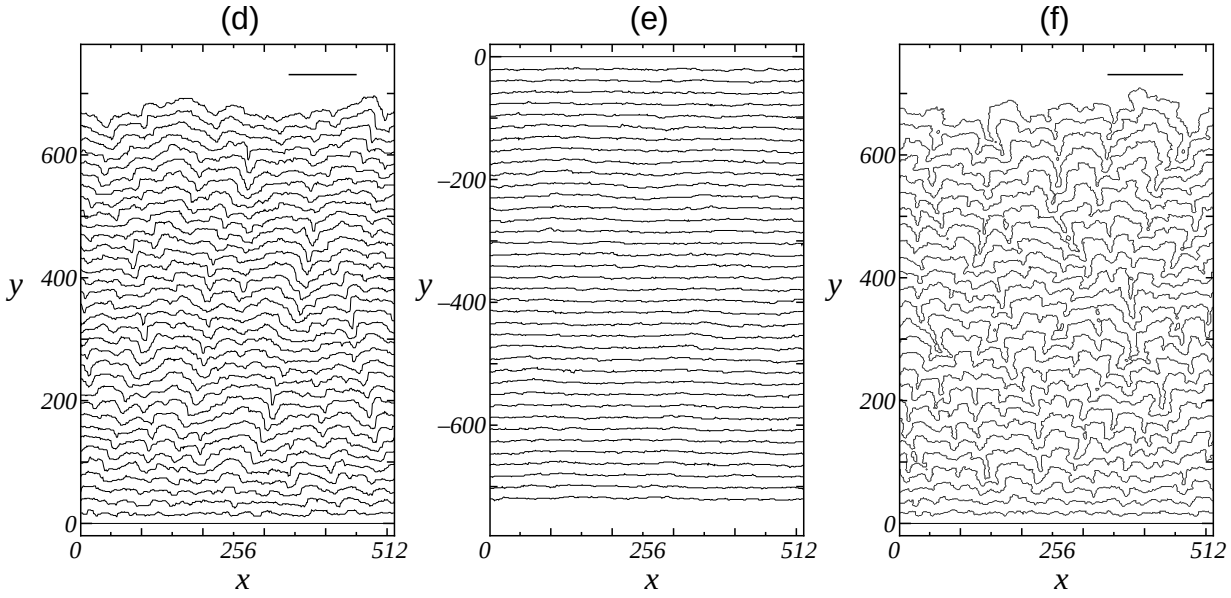

Fig.4(d),(e),(f)

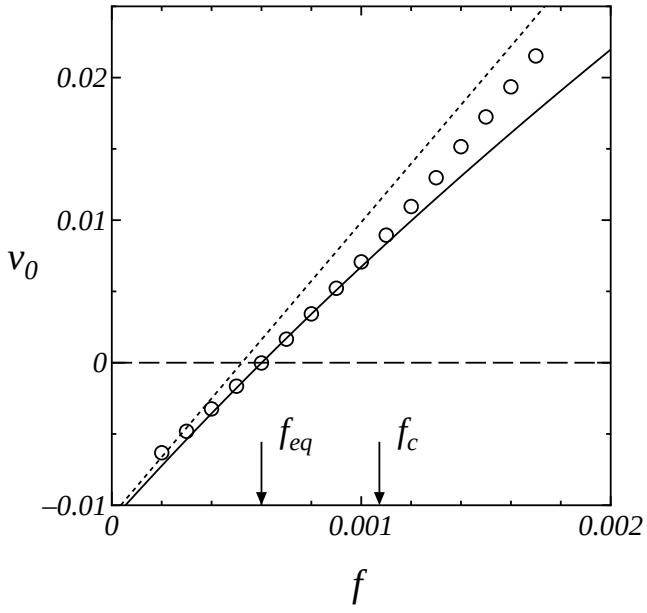

Fig.5

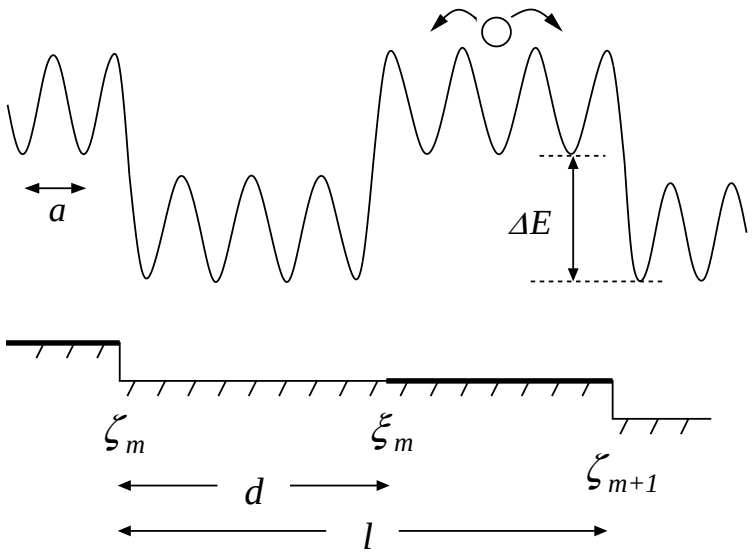
a
ΔE
ζ m
ξ m
ζ m+1
d
l

Fig.6

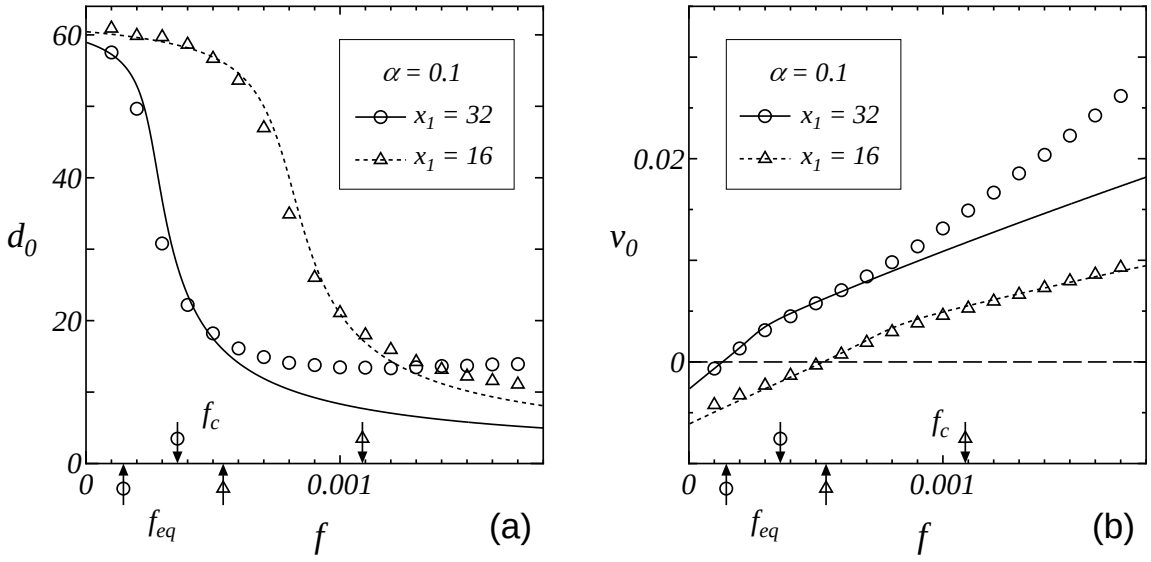
60
40
20
0
d0
α = 0.1
x1 = 32
x1 = 16
fc
feq
0
0.001
f
(a)
0.02
0
v0
α = 0.1
x1 = 32
x1 = 16
fc
feq
0
0.001
f
(b)

Fig.7(a),(b)

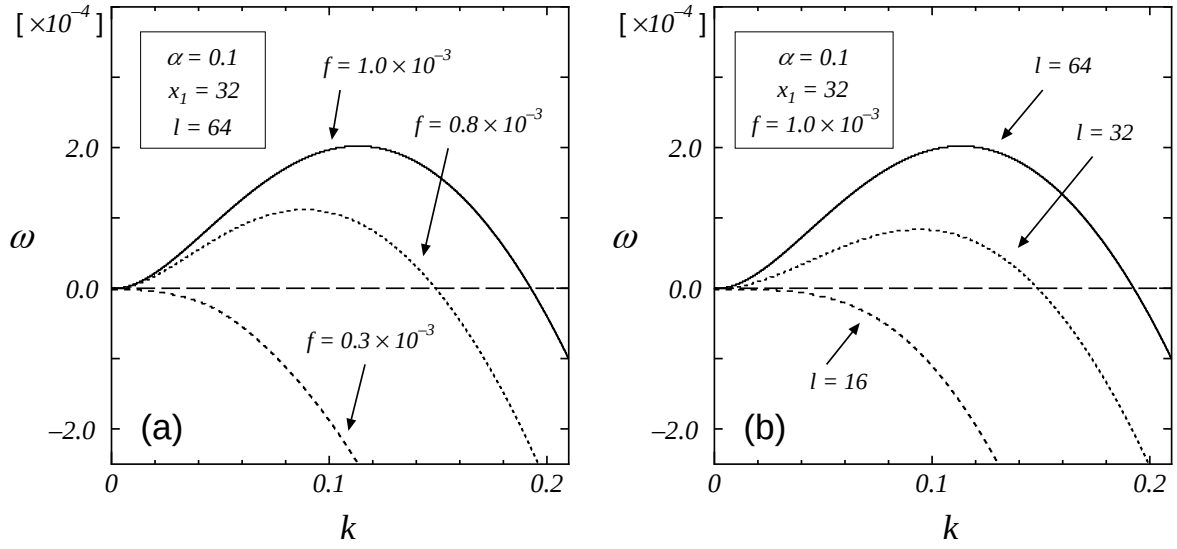
[×10^−4]
α = 0.1
x1 = 32
l = 64
f = 1.0 × 10^−3
f = 0.8 × 10^−3
f = 0.3 × 10^−3
ω
2.0
0.0
−2.0
(a)
0
0.1
0.2
k
[×10^−4]
α = 0.1
x1 = 32
f = 1.0 × 10^−3
l = 64
l = 32
l = 16
ω
2.0
0.0
−2.0
(b)
0
0.1
0.2
k

Fig.8(a),(b)

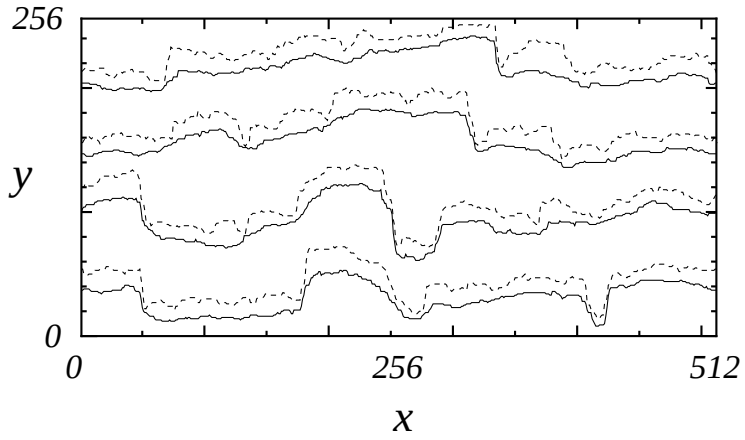
256
y
0
0
256
512
x

Fig.9

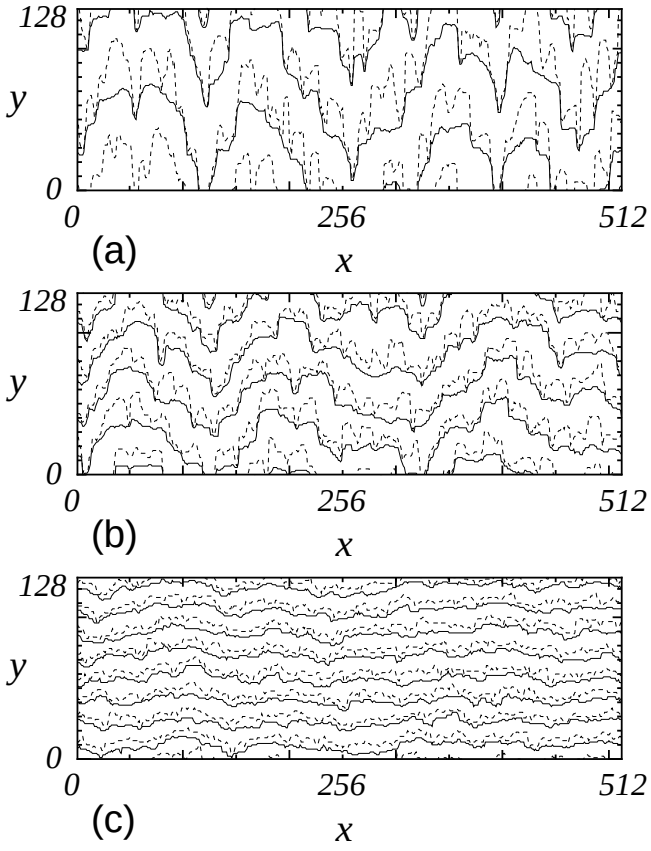

Fig.10(a),(b),(c)

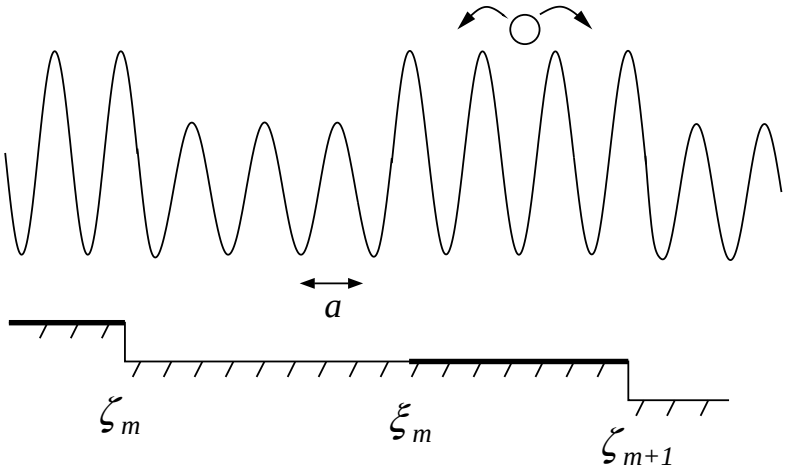

Fig.11

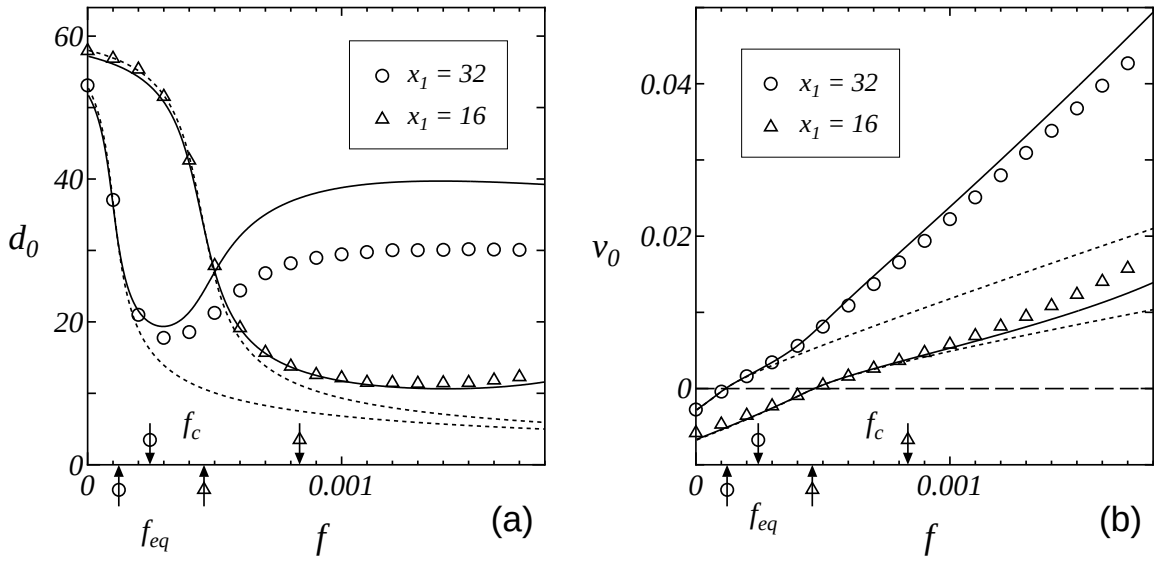

Fig.12(a),(b)

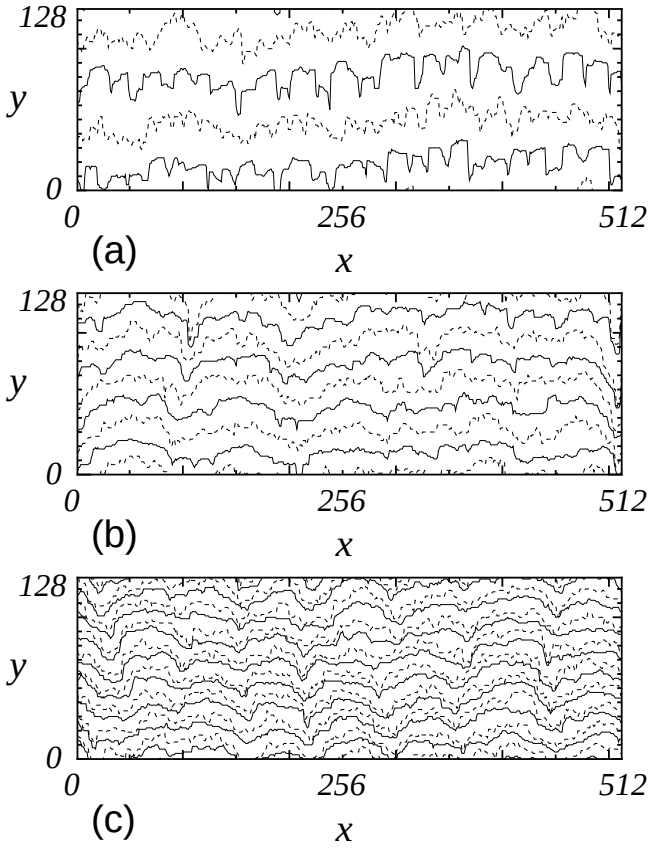

Fig.13(a),(b),(c)

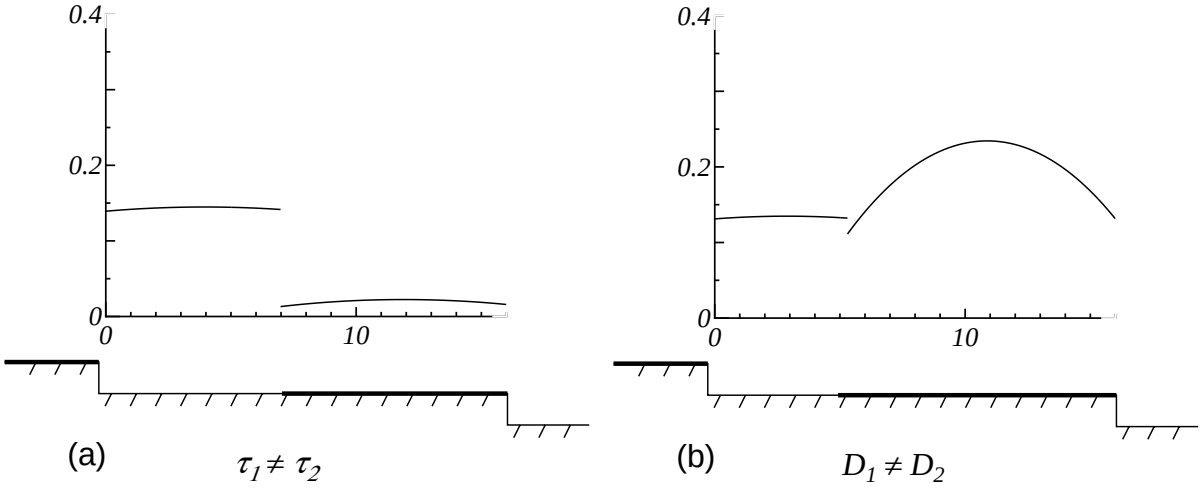

Fig.14(a),(b)